Environmental Science and Pollution Research (2023) 30:27394–27408
https://doi.org/10.1007/s11356-022-24102-5

RESEARCH ARTICLE

Insight into enhanced degradation of tetracycline over peroxymonosulfate activated via biochar-based nanocomposite: performance and mechanism

Tiehong Song[1] · Yanjiao Gao[2] · Jian Ye[3,4,5] · Xin Zhang[2] · Rui Su[2] · Jiacheng Luo[2]

Received: 12 September 2022 / Accepted: 4 November 2022 / Published online: 15 November 2022

Abstract

Rice husk biochars (BCs) doped with ferric chloride were prepared by one-pot method, characterized by SEM, EDS, BET, XRD, and FTIR, and utilized to catalyze peroxymonosulfate (PMS) for tetracycline (TC) degradation. Various influencing factors in the BC/PMS/TC system were investigated, as well as the recycling performance of the optimal BC. The mechanism of BC activation of PMS and degradation of TC were analyzed based on the free radicals quenching experiment and the pathways of TC degradation. The results demonstrated that bBC3 was an excellent catalyst with large specific surface area; the amounts of oxidant and catalyst were important factors affecting the catalytic performance of PMS, while pH had less effect on TC degradation; 10 mM of chloride ions inhibited the TC degradation, while 20 mM promoted the TC degradation; other ions and humic acid inhibited the TC degradation at the set concentrations; activation of PMS by bBC3 yielded species with strong oxidative activity, which were primarily responsible for TC degradation. The bBC3 obtained stable performance for removing TC. This study provided a pathway for the deep utilization of waste rice husks besides an effective method for degrading TC.

Keywords Tetracycline · Biochar · Peroxymonosulfate · Advanced oxidation · Free radicals

Introduction

Tetracycline (TC) is a common antibiotic utilized in aquaculture and veterinary medicine. Due to poor biological utilization, more than 70% of TC are present in the urine and excrement of farmed fish, poultry, and livestock and eventually accumulate in surface water or groundwater through surface runoff or subsurface infiltration (Daghrir and Drogui 2013). The discharge of treated wastewater from waste water treatment plant (WWTP) is also a TC source for surface

Responsible Editor: Guilherme L. Dotto

Highlights
- Peroxymonosulfate activated via biochar doped with $FeCl_3$ facilitates the degradation of tetracycline.
- bBC3 with excellent pore structure exhibits the best tetracycline removal effect.
- Free radicals and non-free radicals are responsible for the oxidation of tetracycline jointly.
- Rice husk biochar applied in advanced oxidation is beneficial to deep utilization of agricultural waste.

✉ Jian Ye
yejian@usc.edu.cn; jnyj1919@hotmail.com

[1] Key Laboratory of Songliao Aquatic Environment, Ministry of Education, Jilin Jianzhu University, Changchun 130118, People's Republic of China

[2] College of Civil Engineering and Architecture, Liaoning University of Technology, Jinzhou 121001, People's Republic of China

[3] School of Resource Environment and Safety Engineering, University of South China, Hengyang 421001, People's Republic of China

[4] Hengyang Key Laboratory of Soil Contamination Control and Remediation, University of South China, Hengyang 421001, People's Republic of China

[5] Hunan Province Engineering Research Center of Radioactive Control Technology in Uranium Mining and Metallurgy, University of South China, Hengyang 421001, People's Republic of China

water. Trace amounts of TC have been detected in various aquatic environments around the world. For examples, the TC concentrations were close to 200 ng/L in surface river and groundwater in China (Dai et al. 2020), as high as 0.11 μg/L in surface water in the UK, 1.2–4.2 μg/L in surface water in Germany (Borghi and Palma 2014), and 0.07–0.37 μg/L in WWTP effluent in the USA (Wang et al. 2021a, b). TC with four basic ring structures in water bodies could not be degraded and volatilized easily (Gopal et al. 2020), and its residues in water sources may endanger drinking water source safety and thereafter threaten human health. Hence, it is necessary to develop effective methods to remove TC from various aquatic environments.

Current biological treatment-based waste water treatment methods are limited in TC removal, thus some advanced oxidation methods were extensively studied, such as ultraviolet/peroxide (UV/H_2O_2) (Jung et al. 2012), ultraviolet/ozone (UV/O_3) (Mishra et al. 2017), ozone/peroxide (O_3/H_2O_2) (Luu and Lee 2014), divalent iron/peroxide (Fe^{2+}/H_2O_2) (Zhang et al. 2019), peroxodisulfate/catalyst (Wu et al. 2022), and peroxymonosulfate/catalyst (Yang et al. 2022). These processes could produce hydroxyl radicals (•OH) and sulfate radicals ($SO_4^{\bullet-}$) with strong oxidative property, which could degrade antibiotics including TC effectively (Wang and Wang 2020). $SO_4^{\bullet-}$ ($E_0 = 2.5–3.1$ V, $t_{1/2} = 30–40$ μs) were confirmed to possess stronger oxidizing potential than that of •OH ($E_0 = 1.9–2.7$ V, $t_{1/2} < 1$ μs), with longer half-life and better selectivity to target pollutants (Zhao et al. 2021). The free radicals generated by peroxymonosulfate (PMS, HSO_5^-) and peroxodisulfate (PDS, $S_2O_8^{2-}$) are mainly $SO_4^{\bullet-}$ under the activation of the catalyst (Song et al. 2019). PMS has an asymmetric structure which is unlike PDS, and its peroxide bond is partially positively charged, making it easier to be approached and activated by nucleophiles (Lee et al. 2020). The main activators include external energy, such as conventional heat (Arvaniti et al. 2022), microwave (Miao et al. 2020), ultrasound (Fedorov et al. 2020), and UV (Chen et al. 2018a), as well as transition metals, such as iron (Fe) (Chen et al. 2020), cobalt (Co) (Zhu et al. 2020), copper (Cu) (Ding et al. 2022), manganese (Mn) (Gao et al. 2021)), and carbon materials (Gao et al. 2022). The energy activation method is relatively expensive and suitable for a small amount of water treatment only. The method of transition metal activation introduces metal ions into water, which may cause secondary pollution easily. However, the carbon material activation method is environmentally friendly and has a good water treatment effect, so it has attracted much attention recently.

Biochar (BC) is produced via thermochemical process of carbonaceous materials (forest residue, agricultural waste, municipal sludge, etc.) (Ghodake et al. 2021) and possess the characteristics of enormous specific surface area, stable thermodynamic and chemical properties, and complex surface functional groups (Ahmed et al. 2016). BC is mainly used for soil remediation or as an adsorbent for organic matter or heavy metals treatment in water (Das et al. 2020). In recent years, it has been studied continuously for its application in catalyzing PDS and PMS. Rong et al. (2019) prepared gamma-iron (III) oxide (γ-Fe_2O_3)/biochar derived from banana and investigated its effect on activating PDS for bisphenol A (BPA) degradation. He et al. (2019) studied the performance of sawdust BC in PDS activation for acid orange 7 (AO7) degradation. Dong et al. (2019) used PDS activated by triiron tetraoxide (Fe_3O_4)/rice husk biochar for diminishing phthalate esters (PAEs) in ocean sediment. Fan et al. (2021) examined and analyzed the capability and mechanism of BPA reduced by sewage sludge BC/PMS system. Jiang et al. (2019) carried out the Fe/BC/PMS process on BPA reduction and elucidated the mechanisms of PMS activation and BPA removal. Zhang et al. (2021) used commercial coconut shell BC in catalyzing PMS for TC decomposition. All studies mentioned above on the activation of PDS and PMS by different sources of BC to degrade various organic compounds provide a good foundation for the application of BC as an activator for advanced oxidation. However, it is found that systematic studies on PMS catalyzed via rice husk BC in decomposing TC are relatively rare.

In this study, one-pot method was introduced to prepare rice husk BCs with different pyrolysis temperatures and ferric chloride doping levels, the structure and composition of the BCs were characterized, their effects on activating PMS and degrading TC were investigated, and the influencing factors and mechanism of the reaction were discussed.

Materials and methods

Materials

The chemical reagents applied in this study are listed in Table 1. The purity of reagents was equal to or higher than analytical grade. Deionized (DI) water was used to dissolve chemicals and prepare solutions of certain concentrations.

Fabrication of BCs

The collected rice husks were first cleaned by DI water for three times and then put into a furnace (60 °C, 24 h) to remove moisture. The dried rice husks were mechanically pulverized, and the rice husk powders of about 60 mesh were screened out for further pyrolysis. The rice husks powders were pyrolyzed for 2 h with nitrogen atmosphere in batches (each batch was 10 g) by using a tube furnace, and the temperature of different batches was kept to be 600℃, 700℃, and 800℃, respectively. Depending on the temperature,

Table 1 Chemical reagents list

Reagent	Molecular formula	Manufacturer
Tetracycline	$C_{22}H_{24}N_2O_8$	McLean Co., Ltd. (Shanghai, China)
Peroxymonosulfate	$H_3K_5O_{18}S_4$	
Methanol	CH_4O	
Humic acid	$C_9H_8Na_2O_4$	
Tert-Butanol	$C_4H_{10}O$	
Ethanol	C_2H_6O	
p-Benzoquinone	$C_6H_4O_2$	
L-Histidine	$C_6H_9N_3O_2$	
Sodium dihydrogen phosphate	NaH_2PO_4	Sinopharm Co., Ltd. (Shanghai, China)
Sodium bicarbonate	Na_2CO_3	
Sodium nitrate	$NaNO_3$	
Sodium chloride	NaCl	
Sodium hydroxide	NaOH	
Sulfuric acid	H_2SO_4	

the obtained BCs were denoted as BC1 (1 = 600℃), BC2 (2 = 700℃), and BC3 (3 = 800℃), respectively.

The rice husk powders (60 mesh, 10 g) were injected into $FeCl_3$ solution (300 mL, 300 mM, or 500 mM) independently. The mixture was agitated for 24 h and clarified for 6 h. After that, the precipitate in the mixture was filtered out and dehydrated. The dried filter residues were pyrolyzed in batches by setting different pyrolysis temperatures. These prepared BCs were named aBC1 (a = 300 mM), aBC2, aBC3, bBC1 (b = 500 mM), bBC2, and bBC3, according to the temperature and the concentration of ferric chloride.

Experimental procedure

Adsorption and degradation of TC

All batch experiments were conducted in 250-mL beakers. Preset numbers of TC, BC, and PMS were added to the beaker to initiate reactions activating PMS and degrading TC. H_2SO_4 (0.1 M) and NaOH (0.1 M) were employed to regulate the pH required for the reaction (pH = 3.0, 6.0, 10.0). The chemical reaction of the mixed solution was carried out at room temperature with magnetic stirring. The sampling times were 10, 20, 30, 60, 120, and 150 min.

Influencing factors

The influencing factors including PMS concentration, bBC3 dosage, TC concentration, and some water quality parameters (pH, Cl^-, HCO_3^-, NO_3^-, $H_2PO_4^-$, HA) on TC degradation were investigated. The experimental procedure was similar as to adsorption and degradation of TC. Taking the degradation experiment as a control experiment, different water quality components were added to the solution to investigate TC degradation.

Table 2 Analytical conditions of HPLC and MS

Instrument	Detection conditions
HPLC	Chromatographic columns: Hypersil GOLD 100 mm × 2.1 mm, 1.9 μm; injection volume, 20.0 μL; column temperature, 30℃; mobile phase, 0.1% formic acid (A), acetonitrile (B)
MS	Ion source: HESI; warp gas rate, 30 mL/min; auxiliary gas rate, 5 mL/min; spray voltage, positive ion 3.0 kV; capillary temperature, 300 °C; S-lens, 50

Free radicals quenching

Different quenchers were added to the system to reveal the oxidative components acting in the reaction of bBC3/PMS/TC system. TBA, EtOH, L–H, and BQ were employed for scavenging •OH, both •OH and $SO_4^{\bullet-}$, $^1O_2$, and $O_2^{\bullet-}$, respectively. The degradation effect of TC was compared between bBC3/PMS/TC systems with and without quencher. According to the inhibition of TC degradation by different quenchers, the oxidative species generated in the bBC3/PMS/TC system were inferred. The experimental procedure was the same as adsorption and degradation of TC.

Experiment of bBC3 recycle

The bBC3-containing solution utilized in the degradation experiment was vacuum filtered to extract the BC and then cleaned with DI water under ultrasonic oscillation. The spent bBC3 was evaporated moisture in oven (60 °C, 24 h) and utilized for bBC3 cycling experiment. The cycle experiment was carried out four times, and removal rates of TC in each time were investigated.

Instrumental analysis

The detection of TC concentrations in batch experiments were achieved via a spectrophotometer (TU-1810, Puxi, China) at 357 nm. TC degradation products were determined by HPLC–MS (Ultimate 3000 UHPLC-Q Exactive, Thermo, USA). The analytical conditions of HPLC and MS are shown in Table 2. The morphology, elemental composition, and main functional groups of various BCs were analyzed by SEM (MERLIN Compact, ZEISS, Germany), EDS (Oxford x-max, ZEISS, Germany), XRD (Ultima IV, Rigaku, Japan), and FTIR (Frontier, Perkin Elmer, America), respectively. The specific surface area and pore size of BCs were surveyed by BET adsorption instrument (ASAP2460, Micromeritics, USA).

Results and discussion

Instrument detection of BCs

The SEM pictures of Fig. 1 show the morphological structures of various BCs. These BCs all formed a porous loose structure. Figure 1a–c exhibit the BCs formed from rice husks at 600℃, 700℃, and 800℃, respectively. Figure 1d–i depict the BCs impregnated with $FeCl_3$ (300 mM, 500 mM). Compared with the BCs not impregnated with $FeCl_3$ (BC1, BC2, BC3), the pores of BCs (aBC1, aBC2, aBC3, bBC1, bBC2, bBC3) became uniformed. According to the detection results of BET adsorption (Table 3), the specific surface area and average pore size of BC3 and bBC3 were larger than other BCs. Both BC3 and bBC3 were formed at a high temperature of 800℃, indicating that elevated temperature promoted the carbonization of rice husks. The specific surface area, average pore size, elemental compositions, and contents of BCs via BET and EDS detection are shown comprehensively in Table 3 and Fig. 2. The main components of BC1, BC2, and BC3 were C, O, and Si. With the increase of preparation temperature, the C proportion increased. In the iron-impregnated BCs, a certain content of Fe was detected except for aBC1. In terms of specific surface area and iron content, bBC3 could be regarded as a favorable adsorption and degradation material. The N_2 isothermal adsorption–desorption curves and pore size distribution of bBC3 are shown in Fig. 3. According to Fig. 3a, the isothermal adsorption curve of bBC3 belonged to type IV isotherm possessing H4 hysteresis loop. Figure 3b showed that the bBC3 had an irregular pore structure and rich in micropores and mes opores.

Figure 4 gives the results of XRD analysis of the crystal structure of BCs. Figure 4a exhibits that BC1, BC2, and BC3 all showing strong peaks at 24°, representing the crystal surface (002) of amorphous carbon (Cazetta et al. 2018). Among these three BCs, BC3 showed the largest peak

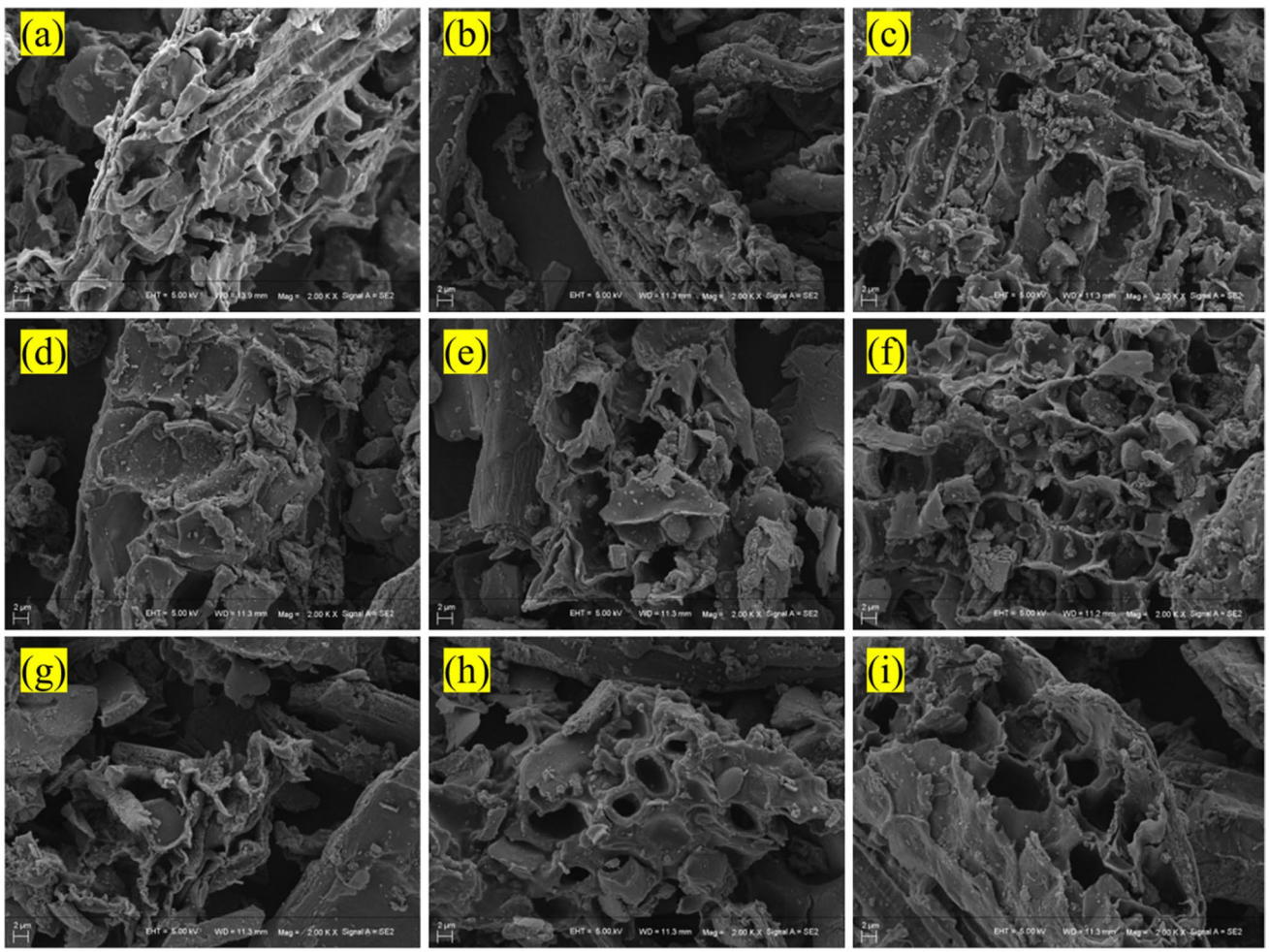

Fig. 1 SEM images of different BCs (2KX). **a** BC1; **b** BC2; **c** BC3; **d** aBC1; **e** aBC2; **f** aBC3; **g** bBC1; **h** bBC2; **i** bBC3

Table 3 Characteristics of BCs

BC	Specific surface area (m^2/g)	Average pore size (nm)	C (% atom)	O (% atom)	Si (% atom)	Fe (% atom)
BC1	79.37	2.64	62.20	25.69	21.12	-
BC2	114.48	2.11	73.39	19.56	7.05	-
BC3	260.41	2.38	81.36	14.71	3.93	-
aBC1	218.67	2.78	85.68	11.92	2.41	-
aBC2	215.16	2.78	65.62	25.32	6.61	2.45
aBC3	214.53	2.80	83.07	11.71	4.23	0.98
bBC1	228.98	2.59	74.23	18.87	5.48	1.42
bBC2	225.01	2.68	85.41	11.56	1.99	1.04
bBC3	264.59	2.68	73.33	19.16	5.45	2.03

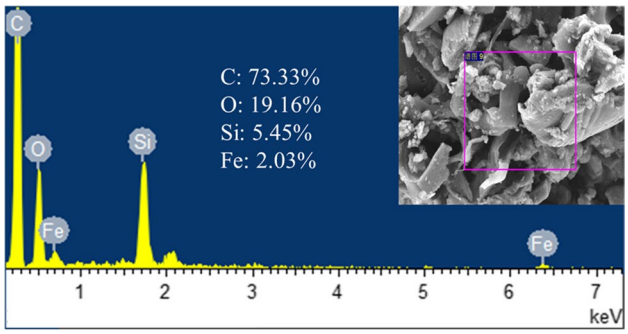

Fig. 2 EDS spectrum of bBC3

intensity, indicating that elevated temperature enhanced the crystallinity of BC. These results were in accord with the increase in carbon content detected by EDS at high temperature. Figure 4b illustrates the difference in diffraction peaks between iron-doped BCs (aBC3, bBC3) and undoped BC (BC3). The inorganic mineral composition Fe_2SiO_4 was detected in the iron-doped BCs. This might be due to the redox reaction between Fe and Si component of rice husks during high temperature pyrolysis.

The functional groups attached to the BCs were analyzed via FTIR, and the spectra are exhibited in Fig. 5. After the rice husk was prepared into BCs at high

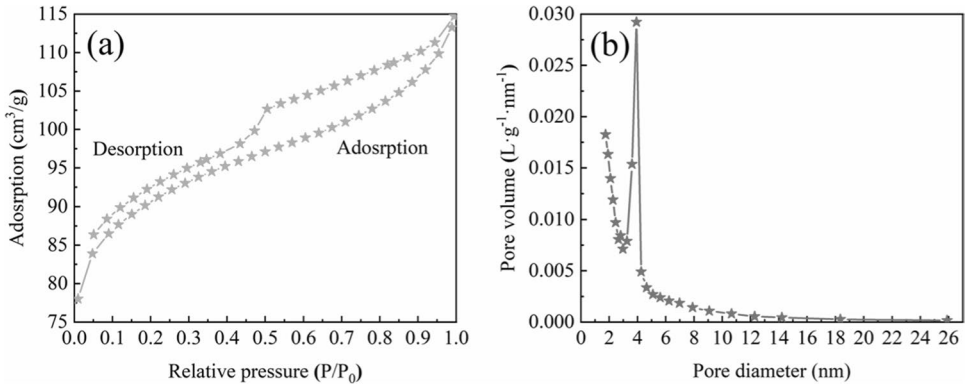

Fig. 3 **a** Isothermal adsorption–desorption curve; **b** aperture distribution curve

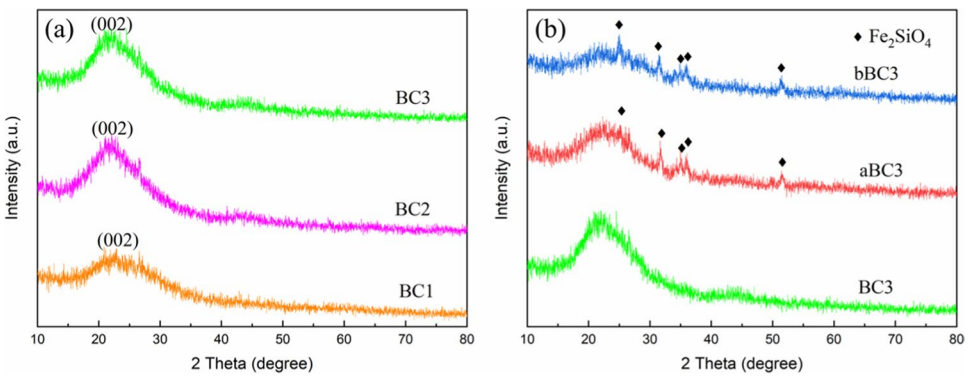

Fig. 4 XRD spectrum of BCs. **a** BC1, BC2, and BC3; **b** BC3, aBC3, and bBC3

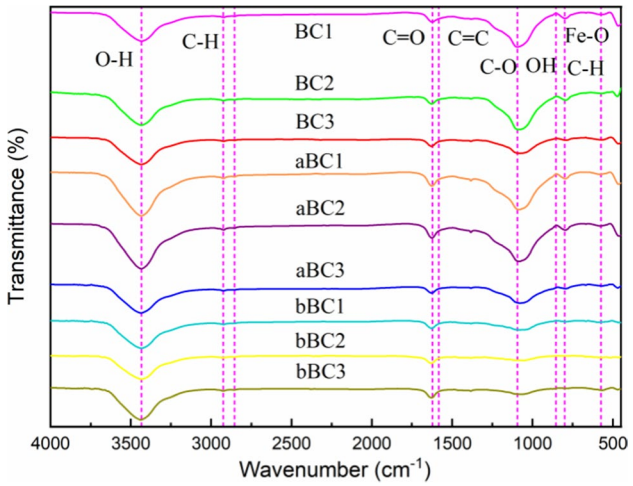

Fig. 5 FTIR spectra of BCs

temperature, abundant functional groups were found growing on BCs. The wavenumber of 3435 cm^{-1} corresponded to hydroxyl O–H (Zhao et al. 2013), and the two bands of 2925 cm^{-1} and 2854 cm^{-1} represented to hydrocarbon C-H (Yuan et al. 2014). The wavenumbers of 1624 cm^{-1},1585 cm^{-1}, and 1095 cm^{-1} indicated the C = O, C = C (Luo et al. 2018), and C-O bonds (Zhang and Wang 2016), respectively. The wavenumbers of 700–830 cm^{-1} represented vibrations outside the plane of the C-H bond (Delgado et al. 2020). The intensity at 574 cm^{-1} expressed the Fe–O bond emerging (Wang et al. 2020a). The C-O content decreased with the increase of the pyrolysis temperature, which was due to the high temperature leading to the volatilization of this functional group. The characteristic peaks of C-H also gradually flattened with pyrolysis temperature increasing, owing to the decomposition or conversion of hydrocarbons into aromatic structures. The appearance of Fe–O bonds indicated that Fe was successfully loaded onto the BCs, and the biochar obtained under higher pyrolysis temperature and higher $FeCl_3$ concentration had a larger bandwidth corresponding to the peak.

Adsorption and degradation of TC by BCs

Figure 6a gives TC removal via various BCs adsorption. Among the undoped BCs (BC1, BC2, BC3), BC3 achieved the highest adsorption removal rate of TC (54.9%) at 150 min. The specific surface area of BC3 prepared at high temperature (800℃) was much larger than that of BC1 (600℃) and BC2 (700℃), so it exhibited a strong ability to adsorb TC. Compared with the undoped BCs, the BCs doped with $FeCl_3$ exhibited a decreasing TC removal rate. The adsorption capacity of bBC3 ($FeCl_3$ 500 mM) to TC was 27.95% only. Therefore, based on the adsorption capacity, BC3 was the optimal material for adsorbing TC. Figure 6b is the TC removal rate vs. time via various BCs/PMS systems. Figure 6b reveals that PMS was able to remove 51.56% of TC within 150 min at room temperature, which indicated that PMS alone also had a certain oxidative ability to TC. However, after adding various BCs to the PMS/TC solution, the TC degradation was further increased. Contrary to the result of the adsorption experiment, the iron-doped BCs achieved better TC degradation rate than the undoped BCs, and bBC3 achieved the best removal effect (94.5%) on TC. This indicated that bBC3 with the highest pyrolysis temperature and the highest concentration of Fe doped had an advantage in degrading TC rather than adsorbing TC. Therefore, bBC3 was used as a catalyst to participate in the reaction of the PMS/TC system in the subsequent experiments on influencing factors and the reuse of BC.

Influencing factors

Figure 7a–d investigated the effects of changes in PMS concentration, BC dosage, TC concentration, and solution pH on TC removal. It was found that among three concentrations of PMS (0.8, 1.6, 3.2 g/L), the highest TC removal rate (94.5%) was obtained at 1.6 g/L (Fig. 7a), indicating that excessive PMS concentration was not conducive to TC degradation. Similar result was obtained in a study of fruit shell derived BC/PMS degradation of TC (Hu et al. 2021). The

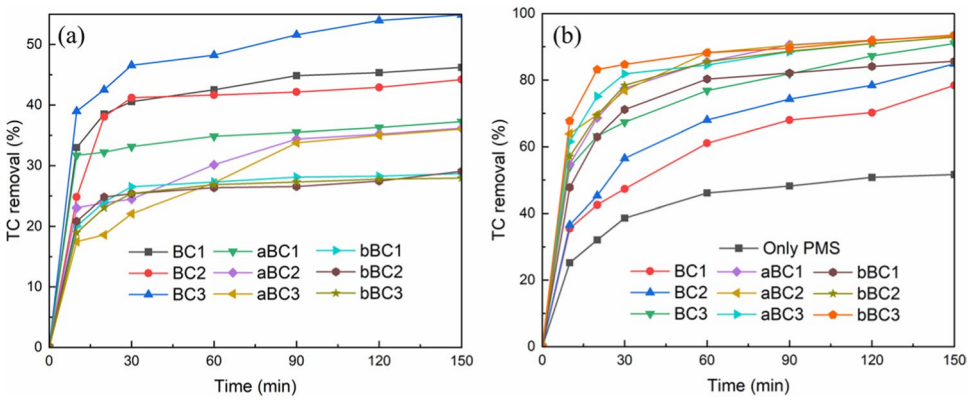

Fig. 6 Adsorption and degradation of TC via BCs. **a** Adsorption; **b** degradation. Conditions: [TC] = 20 mg/L, [BCs] = 1.0 g/L, [PMS] = 1.6 g/L, pH = 6.0

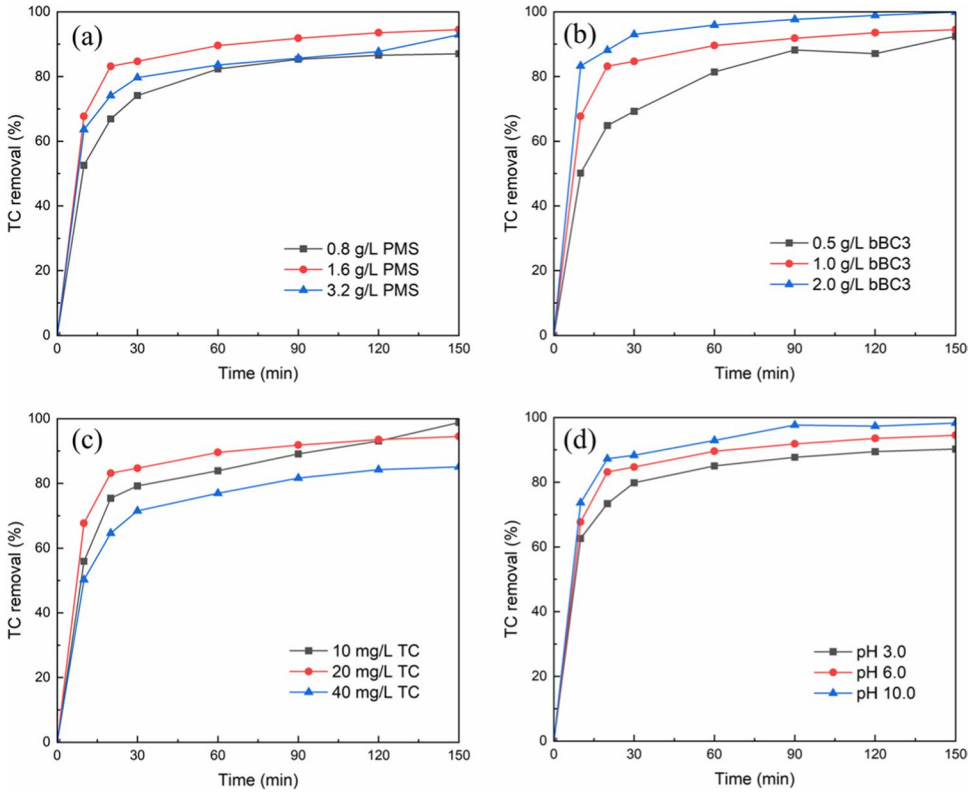

Fig. 7 Effects of **a** PMS concentration, **b** bBC3 amount, **c** TC concentration, and **d** pH on TC removal. Conditions: unless otherwise specified, [bBC3] = 1.0 g/L, [PMS] = 1.6 g/L, [TC] = 20 mg/L, pH = 6.0

reason was that excess PMS may scavenge the already generated free radicals (Eqs. (1)–(2)) (Zhao et al. 2021), so that there were not enough free radicals to oxidize TC. As the bBC3 dosage raised from 0.5 to 2.0 g/L, the TC degradation rate enhanced from 92.5 to 100% within 150 min (Fig. 7b). Increasing the dosage of bBC3 provided more active sites, strengthened the contact between BC and PMS, and activated PMS more efficiently to generate more active species, thereby improving the TC degradation (Hu et al. 2021). Figure 7c displays that the TC degradation rate dropped from 98.8 to 82.1% with TC concentration increasing from 10 to 40 mg/L. Since the dosage of catalyst BC and oxidant PMS did not change as the TC concentration increased, it resulted in a lack of active species for degrading TC in the system (Zhang et al. 2021). Under gradually increasing pH (3.0–10.0), the TC degradation rate also exhibited an upward trend (90.2–98.3%) (Fig. 7d). The removal rate of bBC3/PMS to TC could be maintained above 90% under the three pH conditions, indicating that bBC3/PMS system was less affected by pH in reducing TC. The slight decrease in TC removal rate under acidic conditions might be due to excess H^+ combined with peroxy bond of PMS to form strong hydrogen bonds (Du et al. 2016), accordingly restraining the activation of PMS via bBC3. The degradation rate of TC increased slightly under alkaline conditions, which was attributed to base catalyzing the PMS to generate more oxidizing species (Qi et al. 2016).

$$HSO_5^- + SO_4^{\bullet -} \rightarrow SO_4^{2-} + SO_5^{\bullet -} + H^+ \quad (1)$$

$$HSO_5^- + {}^{\bullet}OH \rightarrow SO_5^{\bullet -} + H_2O \quad (2)$$

Figure 8a–d depict the changes of TC reduction in bBC3/PMS system in the presence of Cl^-, HCO_3^-, NO_3^-, and $H_2PO_4^-$, respectively. Figure 8a shows that the presence of 10-mM Cl^- inhibited the degradation of TC, while 20-mM Cl^- slightly promoted the degradation of TC. The inhibitory effect of low concentration Cl^- was due to Cl^- reacted with active free radicals ($SO_4^{\bullet -}$, •OH) to generate less active free radicals ($Cl^{\bullet}$, $ClOH^{\bullet -}$, $Cl_2^{\bullet -}$) (Eqs. (3)–(6)) (Li et al. 2021). However, the promotion of TC degradation by high concentrations of Cl^- lied in the reaction of Cl^- with HSO_5^- to produce HClO and Cl_2 (Eqs. (7)–(8)) (Liu et al. 2016), which had strong oxidizing properties, thereby assisting $SO_4^{\bullet -}$ and •OH to attack TC. The appearance of HCO_3^- in the F2BC3/PMS system promoted the degradation of TC, and the higher the HCO_3^- concentration was, the greater the promotion effect was (Fig. 8b). The addition of a large amount of HCO_3^- caused the solution to be alkaline, which was beneficial to generate $^1O_2$ with strong oxidative ability in solution (Eqs. (9)–(10)) (Guan et al. 2013), thereby improving TC reduction rate. Both NO_3^- and $H_2PO_4^-$ expressed inhibitory effect on TC reduction (Fig. 8c and d). This was

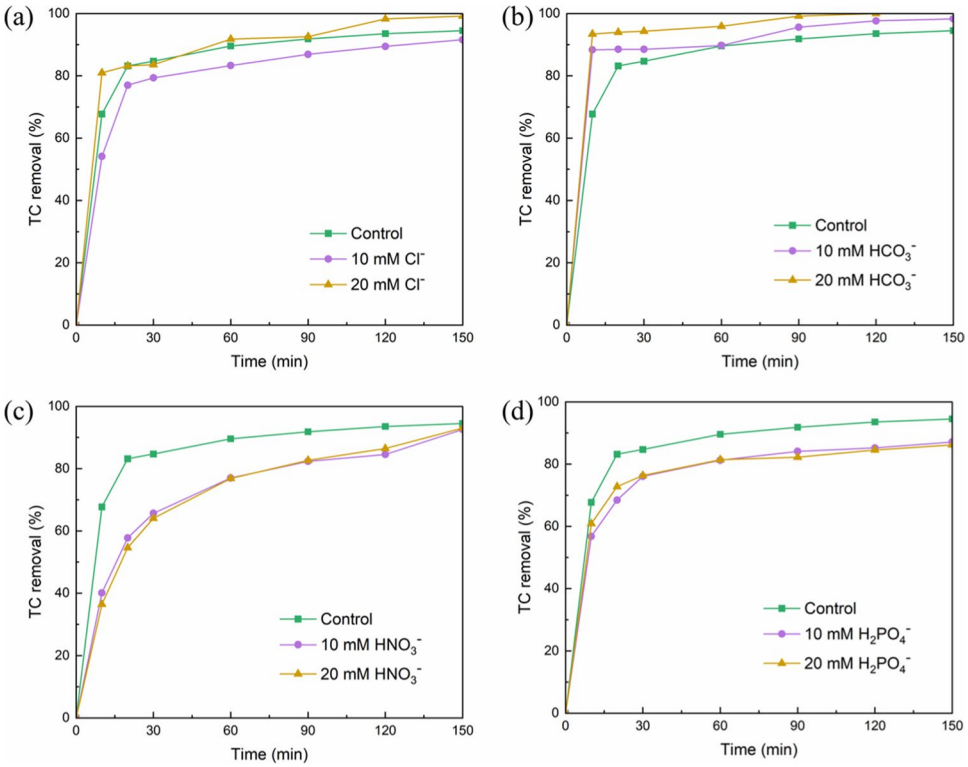

Fig. 8 Effects of **a** Cl- concentration, **b** HCO_3^- concentration, **c** NO_3^- concentration, and **d** $H_2PO_4^-$ concentration on TC removal. Conditions: [bBC3] = 1.0g/L,[PMS] = 1.6g/L, [TC] = 20 mg/L, pH = 6.0

the results of these two ions competed for free radicals with TC (Eqs. (11)–(12)) (Han et al. 2022).

$$SO_4^{\bullet-} + Cl^- \rightarrow SO_4^{2-} + Cl^{\bullet} \quad (3)$$

$$^{\bullet}OH + Cl^- \rightarrow ClOH^{\bullet-} \quad (4)$$

$$ClOH^{\bullet-} + H^+ \rightarrow Cl^{\bullet} + H_2O \quad (5)$$

$$Cl^{\bullet} + Cl^- \rightarrow Cl_2^{\bullet-} \quad (6)$$

$$HSO_5^- + Cl^- \rightarrow SO_4^{2-} + HOCl \quad (7)$$

$$HSO_5^- + 2Cl^- + H^+ \rightarrow SO_4^{2-} + Cl_2 + H_2O \quad (8)$$

$$HSO_5^- + OH^- \rightarrow SO_5^{2-} + H_2O \quad (9)$$

$$HSO_5^- + SO_5^{2-} \rightarrow SO_4^{2-} + HSO_4^- + {}^1O_2 \quad (10)$$

$$SO_4^{\bullet-} + NO_3^- \rightarrow SO_4^{2-} + NO_3^{\bullet} \quad (11)$$

$$SO_4^{\bullet-} + H_2PO_4^- \rightarrow SO_4^{2-} + H_2PO_4^{\bullet} \quad (12)$$

Figure 9 examines the influence of the presence of HA on TC removal since HA is a typical natural organic compound rich in carboxyl and phenolic hydroxyl groups. It can be seen from Fig. 9 that TC degradation in bBC3/PMS/HA system was lower than that in bBC3/PMS system. One reason was that HA, as an organic matter, competed with TC for free radicals, so that there were not enough free radicals to degrade TC (Fu et al. 2019). Another reason might be that

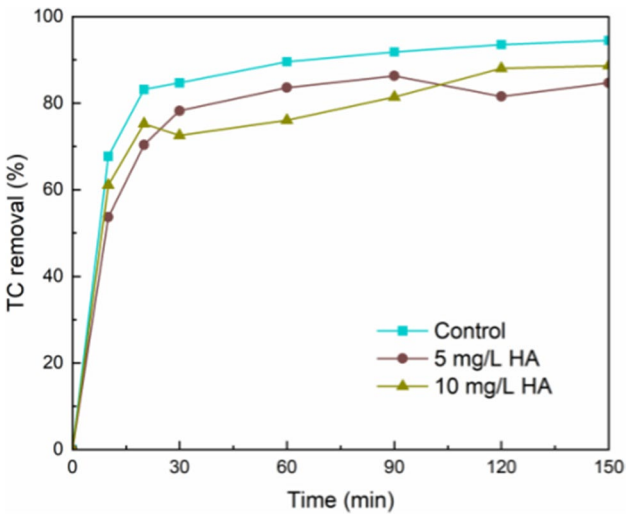

Fig. 9 Effects of HA concentration on TC removal. Conditions: [bBC3] = 1.0 g/L, [PMS] = 1.6 g/L, [TC] = 20 mg/L, pH = 6.0

bBC3 was easy to adsorb HA with carboxyl and phenolic hydroxyl groups (Chen et al. 2018b), which led to the deactivation of the active site of bBC3 as a catalyst so that bBC3 could not catalyze PMS to generate free radicals efficiently.

Performance comparison of various BCs

To evaluate the performance of the bBC3 compared with other BCs in TC degrading in diffident BC/PMS systems, the results from previous studies are shown in Table 4. It was found that bBC3 and most BCs in Table 4 all could achieve above 90% TC removal efficiency. Depending on catalyst dosage, PMS concentration, BPA concentration, pH, temperature, and reaction time, the removal rate of TC was slightly different. Therefore, a better optimization of the reaction conditions would be beneficial to improve the efficiency of TC degradation by different PMS/BCs systems.

Mechanism analysis

Figure 10 depicts the changes of TC degradation rates after TBA, EtOH, L–H, and BQ were added to the bBC3/PMS system. Within 150 min, the degradation rates of TC by the control system and the bBC3/PMS system with TBA, EtOH, L–H, and BQ were 94.50%, 80.95%, 85.35%, 76.83%, and 80.46%, respectively. This result proved that TBA, EtOH, L–H, and BQ all inhibited the TC degradation to different extents and also testified that •OH, $SO_4^{\bullet-}$, $^1O_2$, and $O_2^{\bullet-}$ emerged in the bBC3/PMS system. TBA quenched •OH ($k = 3.8–7.6 \times 10^8$ M^{-1} s^{-1}) (Tang et al. 2020), which decreased the TC removal rate by 13.55% compared to the control system. EtOH captured both•OH ($k = 1.8–2.8 \times 10^9$ M^{-1} s^{-1}) (Tang et al. 2020) and $SO_4^{\bullet-}$ ($k = 1.6–7.7 \times 10^7$ M^{-1} s^{-1}) (Dai et al. 2022), resulting in 9.15% reduction in TC removal. When L–H and BQ reacted with $^1O_2$ ($k = 3.0 \times 10^9$ M^{-1} s^{-1}) (Dai et al. 2022) and

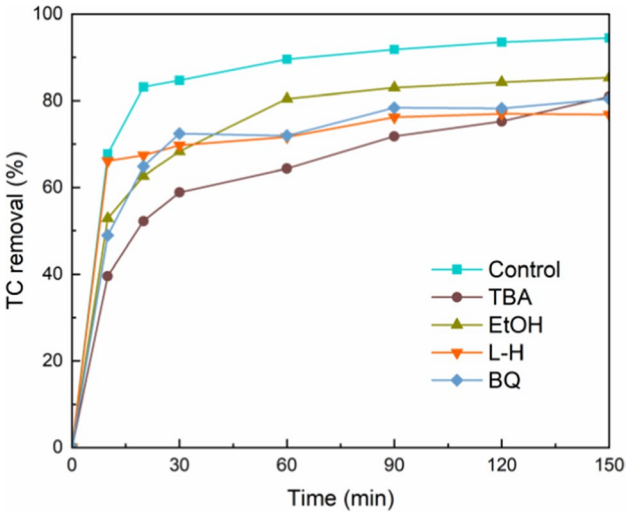

Fig. 10 Effects of TBA, EtOH, L–H, a
nd BQ on TC removal. Conditions: [bBC3] = 1.0 g/L, [PMS] = 1.6 g/L, [TC] = 20 mg/L, pH = 6.0, [EtOH or TBA]:[PMS] = 1000:1, [L–H] = 0.2 M, [BQ] = 5 mM

$O_2^{\bullet-}$($k = 1.0 \times 10^9$ M^{-1} s^{-1}) (Yao et al. 2022) separately, the TC removal rate decreased by 17.67% and 14.04%, respectively. It could be seen that the degradation of TC by bBC3/PMS system involved both free radicals (•OH, $SO_4^{\bullet-}$, and $O_2^{\bullet-}$) and non-radical ($^1O_2$). The contributions of these active species to TC degradation were ranked in descending order as $^1O_2$, $O_2^{\bullet-}$, •OH, and $SO_4^{\bullet-}$.

The intermediate products and degradation routes of TC are shown in Fig. 11. Two pathways interpreted the process of TC degradation. Through the left pathway, TC was first removed hydroxyl group, water molecule, and amino group to convert to P1 (*m/z*) = 396, then P1 was transformed into P3 (*m/z*) = 274 by ring cleavage, and finally P3 was converted into P5 (*m/z*) = 135, P6 (*m/z*) = 110, P7 (*m/z*) = 193,

Table 4 Comparison of tetracycline removal effect with reported BCs

No	Biomass	Reaction systems	Performances	Ref
1	Loofah	$FeSO_4$/BC + PMS	[TC] = 20 mg/L, [PMS] = 0.2 g/L, [$FeSO_4$/BC] = 0.4 g/L, t = 60 min, 90.7% of TC removed	Zhang et al. 2022
2	Tea residue	Fe_3O_4/BC + PMS	[TCH (tetracycline hydrochloride)] = 50 mg/L, [PMS] = 1.0 g/L, [Fe_3O_4/BC] = 1.0 g/L, pH = 7.0, t = 60 min, 97.9% of TCH removed	Wang et al. 2021a, b
3	Spent coffee ground	$CoCl_2$/BC + PMS	[TC] = 0.2 mM, [PMS] = 0.2 mM, [$CoCl_2$/BC] = 0.1 g/L, t = 25 min, T = 25℃, 85.0% of TC removed	Nguyen et al. 2019
4	Piggery sludge	$FeSO_4$-$Fe_2(SO_4)_3$/BC + PMS	[TC] = 10 mg/L, [PMS] = 20 mg/L, [$FeSO_4$-$Fe_2(SO_4)_3$/BC] = 0.5 g/L, pH = 7.0, t = 120 min, 77.2% of TC removed	Luo et al. 2021
5	Passion fruit shell	BC + PMS	[TC] = 20 mg/L, [PMS] = 0.3 g/L, [BC] = 0.4 g/L, pH = 5.4, T = 30℃, t = 120 min, 90.9% of TC removed	Hu et al. 2021
6	Rice husk	$FeCl_3$/BC + PMS	[TC] = 20 mg/L, [PMS] = 1.6 g/L, [bBC3] = 1.0 g/L, pH = 6.0, T = 25℃, t = 150 min, 94.5% of TC removed	This study

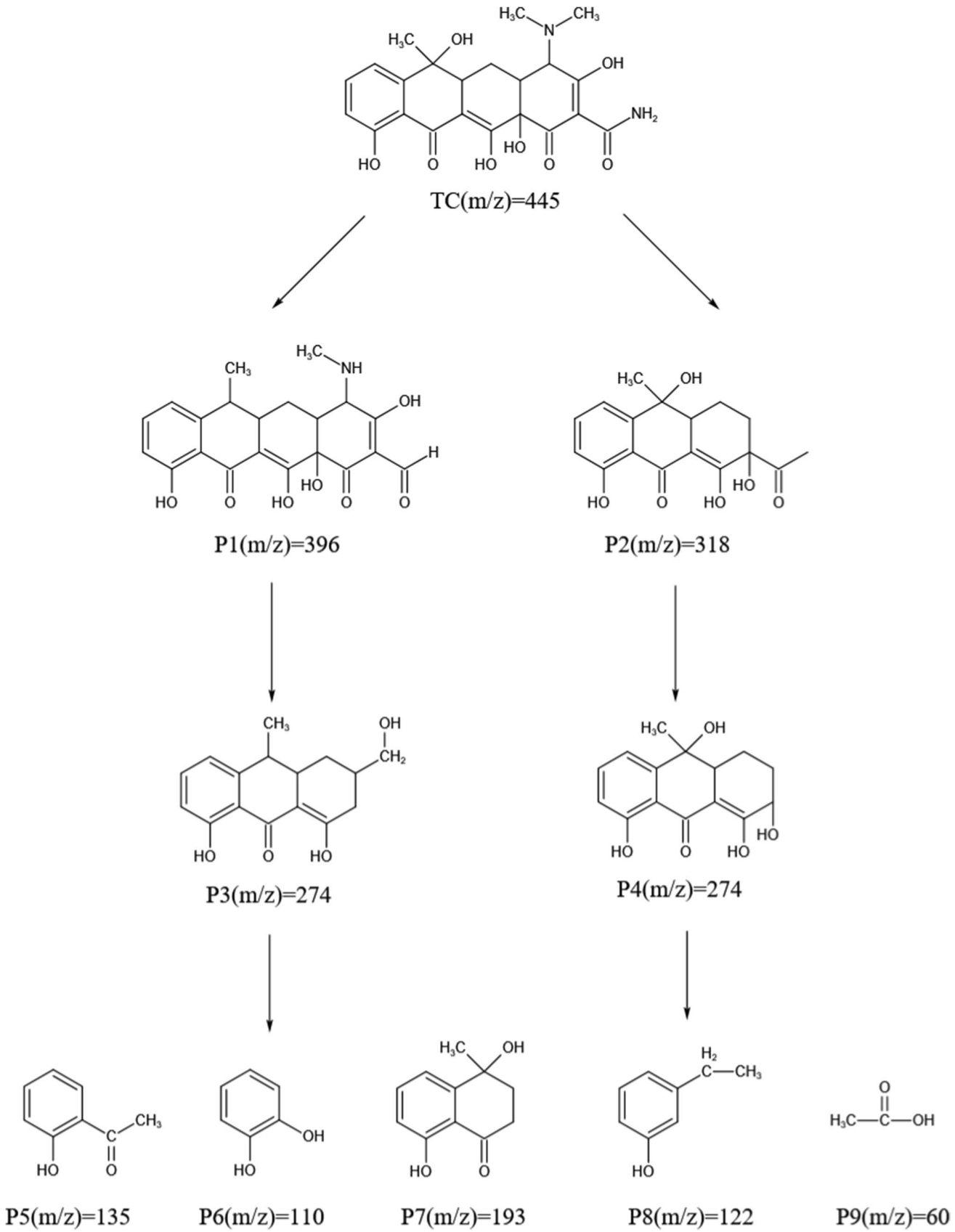

Fig. 11 Degradation pathways and products of TC

P8 (m/z) = 122, and P9 (m/z) = 60. Through the right pathway, the ring of TC was opened first to form P2 (m/z) = 318, then P2 was decarbonylated to obtain P4 (m/z) = 274, and finally P4 was ring-cleaved into P5–P9. Intermediates from both pathways finally were transformed into CO_2 and H_2O.

Figure 12 exhibited the SEM and EDS images of spent bBC3. Compared with the unused bBC3 (Fig. 1i), the surface of the spent bBC3 was rougher, the edge was sharper, and the pores and the surface were filled and attached with impurities. From the table inserted in Fig. 12, the proportion of spent bBC3 was lower than that of unused bBC3, which was due to the precipitation and release of iron in activating PMS in aqueous solution. The changes in the proportion of C and O elements indicated the variation of functional groups attached on bBC3 after catalysis.

Figure 13 reveals the mechanism of bBC3/PMS system in removing TC based on the active species quenching experiment (Fig. 10), analysis of intermediate products and degradation routes of TC (Fig. 11), and the changes in the elemental composition of used bBC3 (Fig. 12). As bBC3 activated PMS, it had the dual ability to donate electrons and accept electrons (Zhao et al. 2021). When PMS gained electrons from bBC3, PMS would generate $SO_4^{\bullet-}$ and •OH (Huong et al. 2020), while when PMS lost electrons, $SO_5^{\bullet-}$ would form, and double $SO_5^{\bullet-}$ could combine to produce $^1O_2$ (Huang et al. 2020). Due to the doping of ferric chloride in bBC3, electron transfer could occur between Fe^{3+} and Fe^{2+} on the bBC3 surface. A part of Fe^{2+} participated in activating PMS, which converted PMS into $SO_4^{\bullet-}$ (Wang et al. 2020b). A series of chain

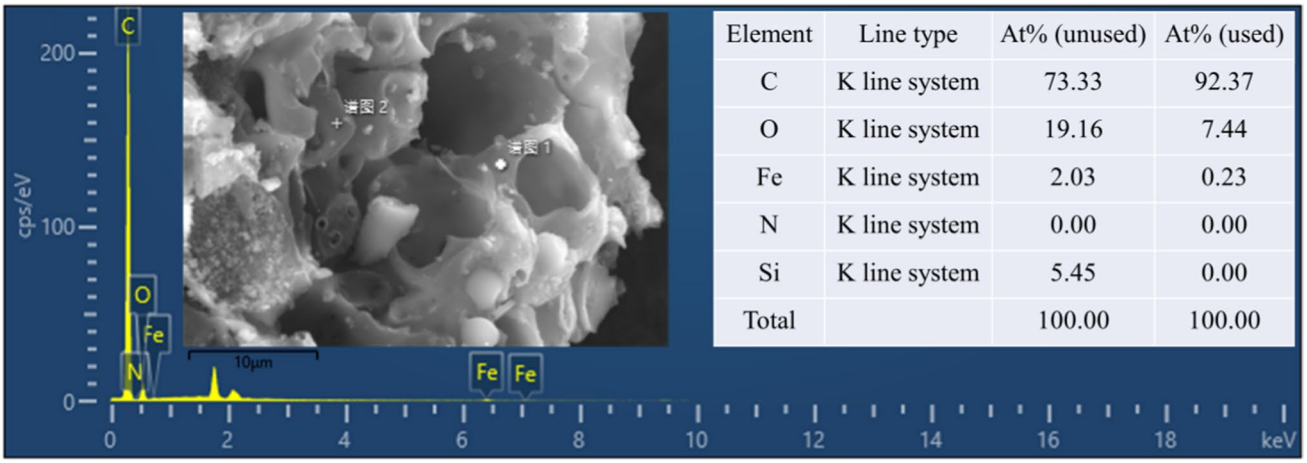

Element	Line type	At% (unused)	At% (used)
C	K line system	73.33	92.37
O	K line system	19.16	7.44
Fe	K line system	2.03	0.23
N	K line system	0.00	0.00
Si	K line system	5.45	0.00
Total		100.00	100.00

Fig. 12 The SEM and EDS images of used bBC3

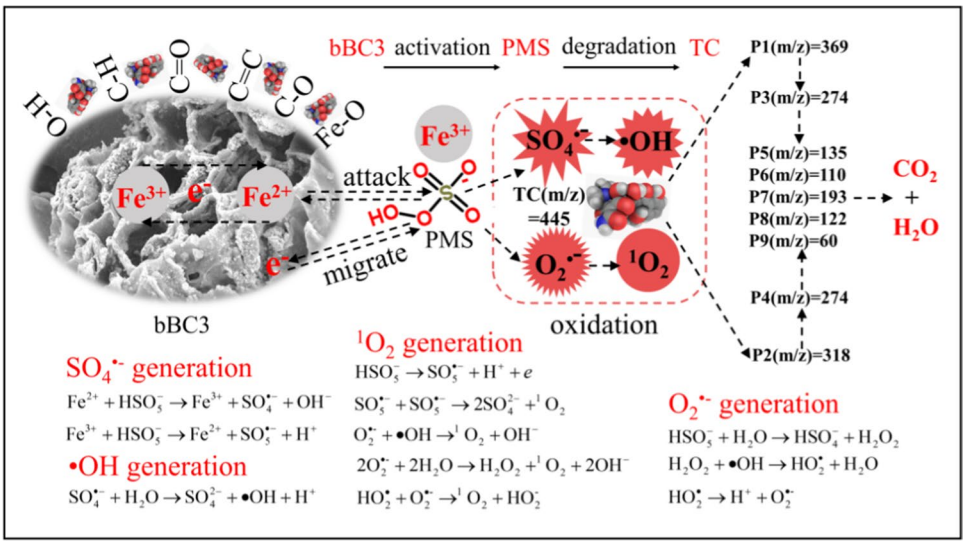

Fig. 13 Mechanism of PMS activation and TC degradation

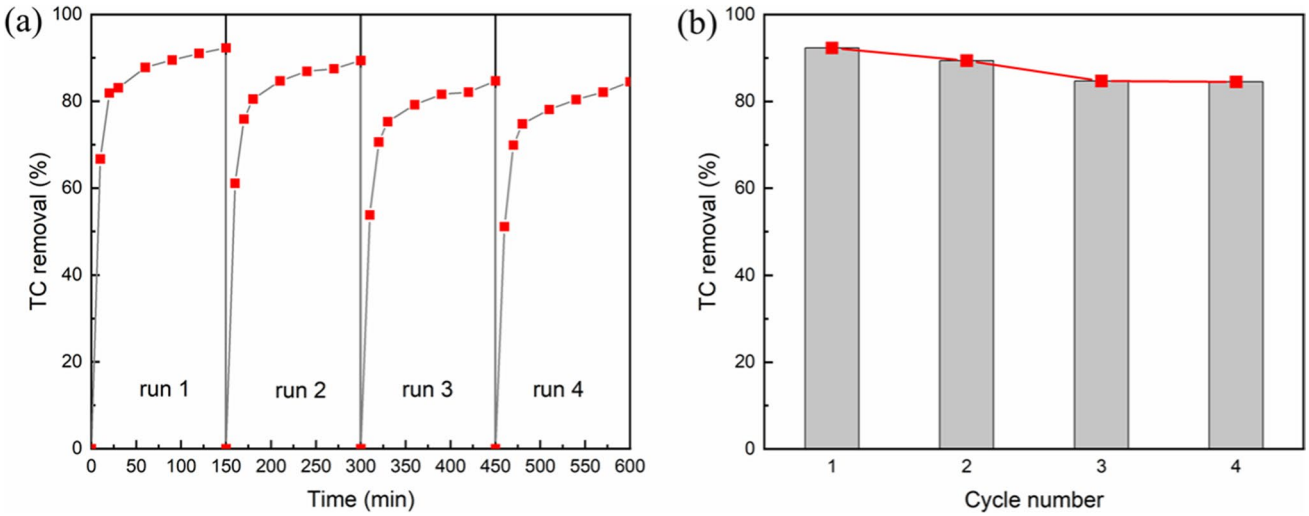

Fig. 14 Degradation pathways and products of TC. **a** Loop experiment; **b** the TC removal corresponding to each run at 50 min

reactions in solution could generate $O_2^{\bullet-}$ (see the equations in Fig. 13). Under the combined action of free radicals (•OH, $SO_4^{\bullet-}$, and $O_2^{\bullet-}$) and non-radical ($^1O_2$), TC was oxidized into a series of intermediates, which ultimately turned into CO_2 and H_2O. As bBC3 activated PMS to degrade TC, the rich pores and large surfaces of bBC3 provided active sites for iron ions to attach and avoid rapid leakage of iron ions into the solution. The oxygen-containing functional groups (O–H, C-O, C = O, OH, and Fe–O) of bBC3 could activate the PMS to remove TC. Moreover, the defect structure of bBC3 could donate the electron to PMS to form •OH or $SO_4^{\bullet-}$. Due to the doping of $FeCl_3$ into the BC, a cycle of Fe^{2+} and Fe^{3+} was formed on the surface of the bBC3, allowing ongoing Fe^{2+} to activate PMS to generate $SO_4^{\bullet-}$. During the reaction, active species such as •OH, $SO_4^{\bullet-}$, $O_2^{\bullet-}$, and $^1O_2$ were formed which played a key role in the degradation of TC. These species were produced by the catalytic effect of bBC3 and Fe^2 on PMS activation. Under the combined effect of these oxygenated species, TC was attacked to degrade into smaller intermediates and finally into CO_2 and H_2O.

bBC3 reuse experiment

Figure 14 exhibits the variation of TC removal in the bBC3/PMS system after four-cycle use of bBC3. The TC degradation in each cycle after 150 min were 92.3%, 89.4%, 84.7%, and 84.5%, respectively. The oxidation of functional groups towards bBC3 and the adhering of degradation products on the bBC3 resulted in the decrease of the specific surface area and active sites of bBC3, which inhibited the activation efficiency of the bBC3 to PMS, and ultimately led to TC degradation suppressed. Although the removal rate of TC decreased in each cycle, it was still above 80%, indicating that the bBC3 had a stable reusability.

Conclusions

In this study, ferric chloride modified BCs were prepared and characterized for activating PMS to degrade TC in aquatic solution. According to the materials analysis and batch experiments, the following conclusions were gained:

(1) BC named bBC3 was proved to have excellent pore structure and substantial oxygen-containing functional groups and obtained the best activation ability on PMS.
(2) The TC degradation in bBC3/PMS system could adapt to various pH (3.0–10.0) range, and the best TC degradation rate was obtained at pH of 10. The increase of the concentration of PMS first enhanced TC removal and then inhibited TC removal. The increase in bBC3 dosage was in favor of TC reduction; however, incremental initial concentration of TC decreased the degradation rate of TC.
(3) Cl^- at low concentration of 10 mM inhibited TC removal, while 20 mM Cl^- assisted TC reduction. The presence of HCO_3^- in solution enhanced the degradation rate of TC, while NO_3^-, $H_2PO_4^-$, and HA suppressed the decomposition of TC, respectively.
(4) TC degraded via bBC3/PMS system was attributed to the synergistic effect of free radicals and non-free radical. Non-free radical species contributed the most to TC degradation.
(5) It was testified that bBC3 had favorable reuse ability, was an economical and effective catalyst in PMS activating.

Author contribution TS: conceptualization, writing—review and editing, supervision. YG: experimental design, writing—original draft preparation. JY: experimental design, data curation, writing—review and editing. XZ: experimental design, formal analysis, data curation. RS: investigation, data curation. JL: investigation, data curation.

Funding This work was comprehensively financially supported by the Education Department of Liaoning Province (JZL202015406), the Natural Science Foundation of Jilin Province (YDZJ202201ZYTS681), and the Outstanding Youth Program of Scientific Research Foundation of Department of Education of Hunan Province (20B505), China.

Data availability Not applicable.

Declarations

Ethics approval Not applicable

Consent to participate Not applicable

Consent for publication Not applicable

Competing interests The authors declare no competing interests.

References

Ahmed MB, Zhou JL, Ngo HH, Guo W (2016) Insight into biochar properties and its cost analysis. Biomass Bioenerg 84:76–86. https://doi.org/10.1016/j.biombioe.2015.11.002

Arvaniti OS, Ioannidi AA, Mantzavinos D, Frontistis Z (2022) Heat-activated persulfate for the degradation of micropollutants in water: a comprehensive review and future perspectives. J Environ Manage 318:115568. https://doi.org/10.1016/j.jenvman.2022.115568

Borghi AA, Palma MSA (2014) Tetracycline: production, waste treatment and environmental impact assessment. Braz J Pharm Sci 50:25–40. https://doi.org/10.1590/S1984-82502011000100003

Cazetta AL, Zhang T, Silva TL, Almeida VC, Asefa T (2018) Bone char-derived metal-free N-and S-co-doped nanoporous carbon and its efficient electrocatalytic activity for hydrazine oxidation. Appl Catal B Environ 225:30–39. https://doi.org/10.1016/j.apcatb.2017.11.050

Chen L, Cai T, Cheng C, Xiong Z, Ding D (2018a) Degradation of acetamiprid in UV/H_2O_2 and UV/persulfate systems: a comparative study. Chem Eng J 351:1137–1146. https://doi.org/10.1016/j.cej.2018.06.107

Chen L, Ding D, Liu C, Cai H, Qu Y, Yang S, Gao Y, Cai T (2018b) Degradation of norfloxacin by $CoFe_2O_4$-GO composite coupled with peroxymonosulfate: a comparative study and mechanistic consideration. Chem Eng J 334:273–284. https://doi.org/10.1016/j.cej.2017.10.040

Chen L, Jiang X, Xie R, Zhang Y, Jin Y, Jiang W (2020) A novel porous biochar-supported Fe-Mn composite as a persulfate activator for the removal of acid red 88. Sep Purif Technol 250:117232. https://doi.org/10.1016/j.seppur.2020.117232

Daghrir R, Drogui P (2013) Tetracycline antibiotics in the environment: a review. Environ Chem Lett 11:209–227. https://doi.org/10.1007/s10311-013-0404-8

Dai Y, Liu M, Li J, Yang S, Sun Y, Sun Q (2020) A review on pollution situation and treatment methods of tetracycline in groundwater. Sep Sci Technol 55:1005–1021. https://doi.org/10.1080/01496395.2019.1577445

Dai C, Li S, Duan Y, Leong KH, Liu S, Zhang Y, Zhou L, Tu Y (2022) Mechanisms and product toxicity of activated carbon/peracetic acid for degradation of sulfamethoxazole: implications for groundwater remediation. Water Res 216:118347. https://doi.org/10.1016/j.watres.2022.118347

Das SK, Ghosh GK, Avasthe R (2020) Application of biochar in agriculture and environment, and its safety issues. Biomass Convers Bior 1:11. https://doi.org/10.1007/s13399-020-01013-4

Delgado F, Gutierrez VS, Dennehy M, Alvarez M (2020) Stable and efficient metal-biochar supported catalyst: degradation of model pollutants through sulfate radical-based advanced oxidation processes. Biochar 2:319–328. https://doi.org/10.1007/s42773-020-00058-y

Ding Y, Fu L, Peng X, Lei M, Wang C, Jiang J (2022) Copper catalysts for radical and nonradical persulfate based advanced oxidation processes: certainties and uncertainties. Chem Eng J 427:131776. https://doi.org/10.1016/j.cej.2021.131776

Dong CD, Chen CW, Hung CM (2019) Persulfate activation with rice husk-based magnetic biochar for degrading PAEs in marine sediments. Environ Sci Pollut Res 26:33781–33790. https://doi.org/10.1007/s11356-018-2423-2

Du Y, Ma W, Liu P, Zou B, Ma J (2016) Magnetic $CoFe_2O_4$ nanoparticles supported on titanate nanotubes ($CoFe_2O_4$/TNTs) as a novel heterogeneous catalyst for peroxymonosulfate activation and degradation of organic pollutants. J Hazard Mater 308:58–66. https://doi.org/10.1016/j.jhazmat.2016.01.035

Fan X, Lin H, Zhao J, Mao Y, Zhang J, Zhang H (2021) Activation of peroxymonosulfate by sewage sludge biochar-based catalyst for efficient removal of bisphenol A: performance and mechanism. Sep Purif Technol 272:118909. https://doi.org/10.1016/j.seppur.2021.118909

Fedorov K, Plata-Gryl M, Khan JA, Boczkaj G (2020) Ultrasound-assisted heterogeneous activation of persulfate and peroxymonosulfate by asphaltenes for the degradation of BTEX in water. J Hazard Mater 397:122804. https://doi.org/10.1016/j.jhazmat.2020.122804

Fu H, Ma S, Zhao P, Xu S, Zhan S (2019) Activation of peroxymonosulfate by graphitized hierarchical porous biochar and $MnFe_2O_4$ magnetic nanoarchitecture for organic pollutants degradation: structure dependence and mechanism. Chem Eng J 360:157–170. https://doi.org/10.1016/j.cej.2018.11.207

Gao Y, Zhou Y, Pang SY, Jiang J, Shen YM, Song Y, Duan JB, Guo Q (2021) Enhanced peroxymonosulfate activation via complexed Mn (II): a novel non-radical oxidation mechanism involving manganese intermediates. Water Res 193:116856. https://doi.org/10.1016/j.watres.2021.116856

Gao Y, Wang Q, Ji G, Li A (2022) Degradation of antibiotic pollutants by persulfate activated with various carbon materials. Chem Eng J 429:132387. https://doi.org/10.1016/j.cej.2021.132387

Ghodake GS, Shinde SK, Kadam AA, Saratale RG, Saratale GD, Kumar M, Palem RR, AL-Shwaiman HA, Elgorban AM, Syed A, Kim DY (2021) Review on biomass feedstocks, pyrolysis mechanism and physicochemical properties of biochar: state-of-the-art framework to speed up vision of circular bioeconomy. J Clean Prod 297:126645. https://doi.org/10.1016/j.jclepro.2021.126645

Gopal G, Alex SA, Chandrasekaran N, Mukherjee A (2020) A review on tetracycline removal from aqueous systems by advanced treatment techniques. RSC Adv 10:27081–27095. https://doi.org/10.1039/D0RA04264A

Guan YH, Ma J, Ren YM, Liu YL, Xiao JY, Lin LQ, Zhang C (2013) Efficient degradation of atrazine by magnetic porous copper ferrite catalyzed peroxymonosulfate oxidation via the formation of hydroxyl and sulfate radicals. Water Res 47:5431–5438. https://doi.org/10.1016/j.watres.2013.06.023

Han Y, Gan L, Gong H, Han J, Qiao W, Xu L (2022) Photoactivation of peroxymonosulfate by wood pulp cellulose biochar/g-C_3N_4

composite for diclofenac degradation: the radical and non-radical pathways. Biochar 4:1–19. https://doi.org/10.1007/s42773-022-00155-0

He J, Xiao Y, Tang J, Chen H, Sun H (2019) Persulfate activation with sawdust biochar in aqueous solution by enhanced electron donor-transfer effect. Sci Total Environ 690:768–777. https://doi.org/10.1016/j.scitotenv.2019.07.043

Huang S, Wang T, Chen K, Mei M, Liu J, Li J (2020) Engineered biochar derived from food waste digestate for activation of peroxymonosulfate to remove organic pollutants. Waste Manage 107:211–218. https://doi.org/10.1016/j.wasman.2020.04.009

Huong PT, Jitae K, Al-Tahtamouni TM, Tri NLM, Kim HH, Cho KH, Lee C (2020) Novel activation of peroxymonosulfate by biochar derived from rice husk toward oxidation of organic contaminants in wastewater. J Water Process Eng 33:101037. https://doi.org/10.1016/j.jwpe.2019.101037

Hu Y, Chen D, Zhang R, Ding Y, Ren Z, Fu M, Cao X, Zeng G (2021) Singlet oxygen-dominated activation of peroxymonosulfate by passion fruit shell derived biochar for catalytic degradation of tetracycline through a non-radical oxidation pathway. J Hazard Mater 419:126495. https://doi.org/10.1016/j.jhazmat.2021.126495

Jiang SF, Ling LL, Chen WJ, Liu WJ, Li DC, Jiang H (2019) High efficient removal of bisphenol A in a peroxymonosulfate/iron functionalized biochar system: mechanistic elucidation and quantification of the contributors. Chem Eng J 359:572–583. https://doi.org/10.1016/j.cej.2018.11.124

Jung YJ, Kim WG, Yoon Y, Kang JW, Hong YM, Kim HW (2012) Removal of amoxicillin by UV and UV/H_2O_2 processes. Sci Total Environ 420:160–167. https://doi.org/10.1016/j.scitotenv.2011.12.011

Lee J, Von Gunten U, Kim JH (2020) Persulfate-based advanced oxidation: critical assessment of opportunities and roadblocks. Environ Sci Technol 54:3064–3081. https://doi.org/10.1021/acs.est.9b07082

Li K, Ma S, Xu S, Fu H, Li Z, Li Y, Liu S, Du J (2021) The mechanism changes during bisphenol A degradation in three iron functionalized biochar/peroxymonosulfate systems: the crucial roles of iron contents and graphitized carbon layers. J Hazard Mater 404:124145. https://doi.org/10.1016/j.jhazmat.2020.124145

Liu Y, Guo H, Zhang Y, Tang W, Cheng X, Liu H (2016) Activation of peroxymonosulfate by $BiVO_4$ under visible light for degradation of rhodamine B. Chem Phys Lett 653:101–107. https://doi.org/10.1016/j.cplett.2016.04.069

Luo M, Lin H, Li B, Dong Y, He Y, Wang L (2018) A novel modification of lignin on corncob-based biochar to enhance removal of cadmium from water. Bioresource Technol 259:312–318. https://doi.org/10.1016/j.biortech.2018.03.075

Luo X, Shen M, Liu J, Ma Y, Gong B, Liu H, Huang Z (2021) Resource utilization of piggery sludge to prepare recyclable magnetic biochar for highly efficient degradation of tetracycline through peroxymonosulfate activation. J Clean Prod 294:126372. https://doi.org/10.1016/j.jclepro.2021.126372

Luu HT, Lee K (2014) Degradation and changes in toxicity and biodegradability of tetracycline during ozone/ultraviolet-based advanced oxidation. Water Sci Technol 70:1229–1235. https://doi.org/10.2166/wst.2014.350

Miao D, Zhao S, Zhu K, Zhang P, Wang T, Jia H, Sun H (2020) Activation of persulfate and removal of ethyl-parathion from soil: effect of microwave irradiation. Chemosphere 253:126679. https://doi.org/10.1016/j.chemosphere.2020.126679

Mishra NS, Reddy R, Kuila A, Rani A, Mukherjee P, Nawaz A, Pichiah S (2017) A review on advanced oxidation processes for effective water treatment. Current World Environ 12:470. https://doi.org/10.12944/CWE.12.3.02

Nguyen VT, Nguyen TB, Chen CW, Hung CM, Huang CP, Dong CD (2019) Cobalt-impregnated biochar (Co-SCG) for heterogeneous activation of peroxymonosulfate for removal of tetracycline in water. Bioresource Technol 292:121954. https://doi.org/10.1016/j.biortech.2019.121954

Qi C, Liu X, Ma J, Lin C, Li X, Zhang H (2016) Activation of peroxymonosulfate by base: implications for the degradation of organic pollutants. Chemosphere 151:280–288. https://doi.org/10.1016/j.chemosphere.2016.02.089

Rong X, Xie M, Kong L, Natarajan V, Ma L, Zhan J (2019) The magnetic biochar derived from banana peels as a persulfate activator for organic contaminants degradation. Chem Eng J 372:294–303. https://doi.org/10.1016/j.cej.2019.04.135

Song W, Li J, Wang Z, Zhang X (2019) A mini review of activated methods to persulfate-based advanced oxidation process. Water Sci Technol 79:573–579. https://doi.org/10.2166/wcc.2018.168

Tang S, Tang J, Yuan D, Wang Z, Zhang Y, Rao Y (2020) Elimination of humic acid in water: comparison of UV/PDS and UV/PMS. RSC Adv 10:17627–17634. https://doi.org/10.1039/D0RA01787F

Wang J, Wang S (2020) Reactive species in advanced oxidation processes: Formation, identification and reaction mechanism. Chem Eng J 401:126158. https://doi.org/10.1016/j.cej.2020.126158

Wang H, Xiao K, Yang J, Yu Z, Yu W, Xu Q, Wu Q, Liang S, Hu J, Hou H, Liu B (2020a) Phosphorus recovery from the liquid phase of anaerobic digestate using biochar derived from iron- rich sludge: a potential phosphorus fertilizer. Water Res 174:115629. https://doi.org/10.1016/j.watres.2020.115629

Wang S, Xu W, Wu J, Gong Q, Xie P (2020b) Improved sulfamethoxazole degradation by the addition of MoS_2 into the Fe^{2+}/peroxymonosulfate process. Sep Purif Technol 235:116170. https://doi.org/10.1016/j.seppur.2019.116170

Wang J, Liu X, Yang M, Han H, Zhang S, Ouyang G, Han R (2021a) Removal of tetracycline using modified wheat straw from solution in batch and column modes. J Mol Liq 338:116698. https://doi.org/10.1016/j.molliq.2021.116698

Wang Q, Shi Y, Lv S, Liang Y, Xiao P (2021b) Peroxymonosulfate activation by tea residue biochar loaded with Fe_3O_4 for the degradation of tetracycline hydrochloride: performance and reaction mechanism. RSC Adv 30:18525–18538. https://doi.org/10.1039/D1RA01640G

Wu Z, Tong Z, Xie Y, Sun H, Gong X, Qin P, Liang Y, Yuan X, Zou D, Jiang L (2022) Efficient degradation of tetracycline by persulfate activation with Fe, Co and O co doped g-C_3N_4: performance, mechanism and toxicity. Chem Eng J 434:134732. https://doi.org/10.1016/j.cej.2022.134732

Yao B, Chen X, Zhou K, Luo Z, Li P, Yang Z, Zhou Y (2022) p-Arsanilic acid decontamination over a wide pH range using biochar-supported manganese ferrite material as an effective persulfate catalyst: performances and mechanisms. Biochar 4:1–13. https://doi.org/10.1007/s42773-022-00158-x

Yang Q, Yan Y, Yang X, Liao G, He J, Wang D (2022) The effect of complexation with metal ions on tetracycline degradation by $Fe^{2+}/^{3+}$ and Ru^{3+} activated peroxymonosulfate. Chem Eng J 429:132178. https://doi.org/10.1016/j.cej.2021.132178

Yuan H, Lu T, Wang Y, Huang H, Chen Y (2014) Influence of pyrolysis temperature and holding time on properties of biochar derived from medicinal herb (radix isatidis) residue and its effect on soil CO_2 emission. J Anal Appl Pyrol 110:277–284. https://doi.org/10.1016/j.jaap.2014.09.016

Zhang J, Wang Q (2016) Sustainable mechanisms of biochar derived from brewers' spent grain and sewage sludge for ammonia-nitrogen capture. J Clean Prod 112:3927–3934. https://doi.org/10.1016/j.jclepro.2015.07.096

Zhang N, Chen J, Fang Z, Tsang EP (2019) Ceria accelerated nanoscale zerovalent iron assisted heterogenous Fenton oxidation of tetracycline. Chem Eng J 369:588–599. https://doi.org/10.1016/j.cej.2019.03.112

Zhang W, Yan L, Wang Q, Li X, Guo Y, Song W, Li Y (2021) Ball milling boosted the activation of peroxymonosulfate by biochar for tetracycline removal. J Environ Chem Eng 9:106870. https://doi.org/10.1016/j.jece.2021.106870

Zhang D, Sun J, Li Q, Song H, Xia D (2022) Cu-Doped magnetic loofah biochar for tetracycline degradation via peroxymonosulfate activation. New J Chem 46:17223–17234. https://doi.org/10.1039/D2NJ02885A

Zhao L, Cao X, Mašek O, Zimmerman A (2013) Heterogeneity of biochar properties as a function of feedstock sources and production temperatures. J Hazard Mater 256:1–9. https://doi.org/10.1016/j.jhazmat.2013.04.015

Zhao C, Shao B, Yan M, Liu Z, Liang Q, He Q, Wu T, Liu Y, Pan Y, Huang J, Wang J, Liang J, Tang L (2021) Activation of peroxymonosulfate by biochar-based catalysts and applications in the degradation of organic contaminants: a review. Chem Eng J 416:128829. https://doi.org/10.1016/j.cej.2021.128829

Zhu S, Xu Y, Zhu Z, Liu Z, Wang W (2020) Activation of peroxymonosulfate by magnetic Co-Fe/SiO_2 layered catalyst derived from iron sludge for ciprofloxacin degradation. Chem Eng J 384:123298. https://doi.org/10.1016/j.cej.2019.123298